Title

BiVO4—Liquid Junction Photovoltaic Cell with 0.2% Solar Energy Conversion Efficiency

Journal

Journal of the American Chemical Society, 145(47)

ISSN

0002-7863

Authors

Daemi, Sahar

Kaushik, Samhita

Das, Soumik

et al.

Publication Date

2023-11-29

DOI

10.1021/jacs.3c09546

Peer reviewed

A $BiVO_4$ - liquid junction photovoltaic cell with 0.2% solar energy conversion efficiency

Sahar Daemi, [a] Samhita Kaushik, [b] Soumik Das, [b] Thomas W. Hamann, [b*] Frank E. Osterloh [a*]

[a] Department of Chemistry, University of California, Davis, CA 95616, USA, orcid.org/ 0000-0002-9288-3407 (fosterloh@ucdavis.edu)

[b] Department of Chemistry, Michigan State University, East Lansing, Michigan 48824-1322, United States; orcid.org/0000-0001-6917-7494 (hamann@chemistry.msu.edu)

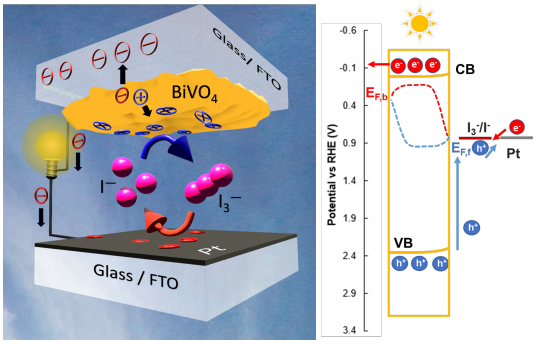

Abstract

$BiVO_4$ is an important photoanode material for water oxidation, but its photoelectrochemistry regarding the triiodide/iodide redox couple is not well understood. Here, we use a combination of open circuit potential measurements, photoelectrochemical scans, and liquid surface photovoltage spectroscopy (SPS) to confirm that $BiVO_4$/triiodide/iodide electrolyte contacts produce up to 0.55 V photovoltage under 23 mW/cm^{-2} illumination from a 470 nm LED. Inspired by these results, we

construct In/FTO/$BiVO_4$/$KI(I_2)_{aq}$/Pt sandwich photoelectrochemical cells from electrochemically grown 0.5 x 0.5 cm^2 $BiVO_4$ and Mo-doped $BiVO_4$ films. Under AM 1.5 illumination, the devices have up to 0.22 % energy conversion efficiency, 0.32 V photovoltage, and 1.8 mA cm^{-2} photocurrent. Based on SPS, hole transfer to iodide is sufficiently fast to prevent the competing water oxidation reaction. Mo-doping increases the IPCE to up to 55% (at 425 nm under front illumination) by improving the $BiVO_4$ conductivity, but this comes at the expense of a lower photovoltage resulting from recombination at the Mo defects, and a detrimental Schottky junction at the interface with FTO. Additional photovoltage losses are caused by the offset between the $BiVO_4$ valence band edge and the triiodide/iodide electrochemical potential, and by electron back transfer to iodide at the FTO back contact (shunting). Overall, this work provides the first example of a $BiVO_4$-liquid photovoltaic cell and an analysis of its limitations. Even though the larger band gaps of metal oxides constrain their solar energy conversion efficiency, their transparency to visible light and deep valence bands make them suitable for tandem photovoltaic devices.

Introduction

Bismuth vanadate ($BiVO_4$) is used widely as a photoanode material in photoelectrochemical cells and in photocatalysts for the water oxidation reaction, a key step in the production of renewable fuels from solar energy [1-6] The visible light driven water oxidation capability of $BiVO_4$ is rooted in its electronic structure. Because the Bi s orbitals participate in bonding, the valence band edge in $BiVO_4$ is more reducing than in other 3d transition metal compounds, and the band gap is smaller (2.4 eV). [7-8] While uses of $BiVO_4$ for the photoelectrochemical oxidization of water, and of organic compounds, [9] sulfite, [10] methanol, [11] or H_2O_2, [12] are well documented in the literature, its photoelectrochemistry with reversible redox couples, such as hexacyanoferrate, [13-14] Fe^{3+}/Fe^{2+}, [5] and IO_3^-/iodide is less established. [15-16] The redox chemistry with iodide would be of particular interest because the triiodide/iodide redox couple is often employed as a redox mediator in dye sensitized solar cells. [17]

$$I_3^- + 2\ e^- \leftrightarrow 3\ I^- \qquad (1)$$

In 2008, Kisch and coworkers reported that $BiVO_4$ electrodes can oxidize iodide with an ICPE of 4% at 420 nm and 1.64 V RHE applied potential. [18] Theoretically, iodide oxidation with $BiVO_4$ does not require any applied bias because the standard reduction potential of the I_3^-/I^- couple (E^0=0.536 V vs NHE) [19] lies ~2.0 eV above the $BiVO_4$ valence band edge. To test this hypothesis, we have studied the photoelectrochemistry of the $BiVO_4$ in the presence of iodide using open circuit potential and liquid surface photovoltage measurements. We confirm that $BiVO_4$ promotes iodide to triiodide oxidation under illumination and without applied bias, and that a rectifying $BiVO_4$ – triiodide/iodide junction is formed that can be used for the fabrication of a solid-liquid photovoltaic cell. The solar cells were characterized with a combination of J-V scans, photovoltage decay, and photoaction spectra. We find that PV performance is limited by several factors, incl.

the 2.4 eV band gap of $BiVO_4$, the energy mismatch between the $BiVO_4$ valence band edge and the iodide oxidation potential, a detrimental junction at the FTO/Mo:$BiVO_4$ interface, poor electron transport throughout the $BiVO_4$ films, and electron back transfer to iodide at the FTO substrate. Remarkably, analysis of the photovoltage of the device shows that water oxidation is completely suppressed in the presence of iodide. These findings not only provide a better understanding of the photoelectrochemistry of $BiVO_4$, but they also demonstrate the possibility of metal oxide-liquid solar cells with aqueous redox couples. The only other examples of such cells date back to 1975, when Mavroides et al [20] reported a TiO_2 photogalvanic cell based on the O_2/H_2O redox couple. Here, O_2 was produced by water oxidation at the TiO_2 photoanode and reduced back to water at the Pt counter electrode. The device generated a V_{OC} of 0.52 V and a I_{SC} of 2.5 cm^{-2} under 150 W Xe lamp illumination and had an external quantum efficiency of 82% at 4.0 eV. [20] A related device was demonstrated by Bard's group in 1976. [21] It had a V_{OC} of 0.90 V and an I_{SC} of 8 mA cm^{-2} under UV illumination from a 450 W Xe lamp. The solar energy conversion efficiency of these devices was never determined, and but likely does not exceed the performance of the $BiVO_4$ device shown here, because of the large band gap of TiO_2 (3.0 eV).

Results and Discussion

$BiVO_4$ and Mo-doped $BiVO_4$ films of 1.0 cm^2 area size were grown on FTO substrates using the well-known electrodeposition/annealing protocol by Choi and coworkers.[22] Selected properties of these films are shown in **Figure 1**. XRD patterns confirm the monoclinic structure of the material, and SEM images confirm the nanostructured morphology of the films (**Figure 1** and **S1**). As shown in **Figure S2**, the Mo concentration in the 1% doped $BiVO_4$ films remained below the detection

limit of Energy dispersive spectroscopy (EDS). Cross section SEM images of $BiVO_4$ films (**Figure 1 and S3**) reveal thicknesses of ~ 1.4 µm and 0.8 µm, respectively, depending on the electrodeposition time. Optical absorption spectra (**Figure 1 and S4**) reveal a 2.5 eV band gap, regardless of Mo doping, slightly above the reported 2.4 eV value. [23]

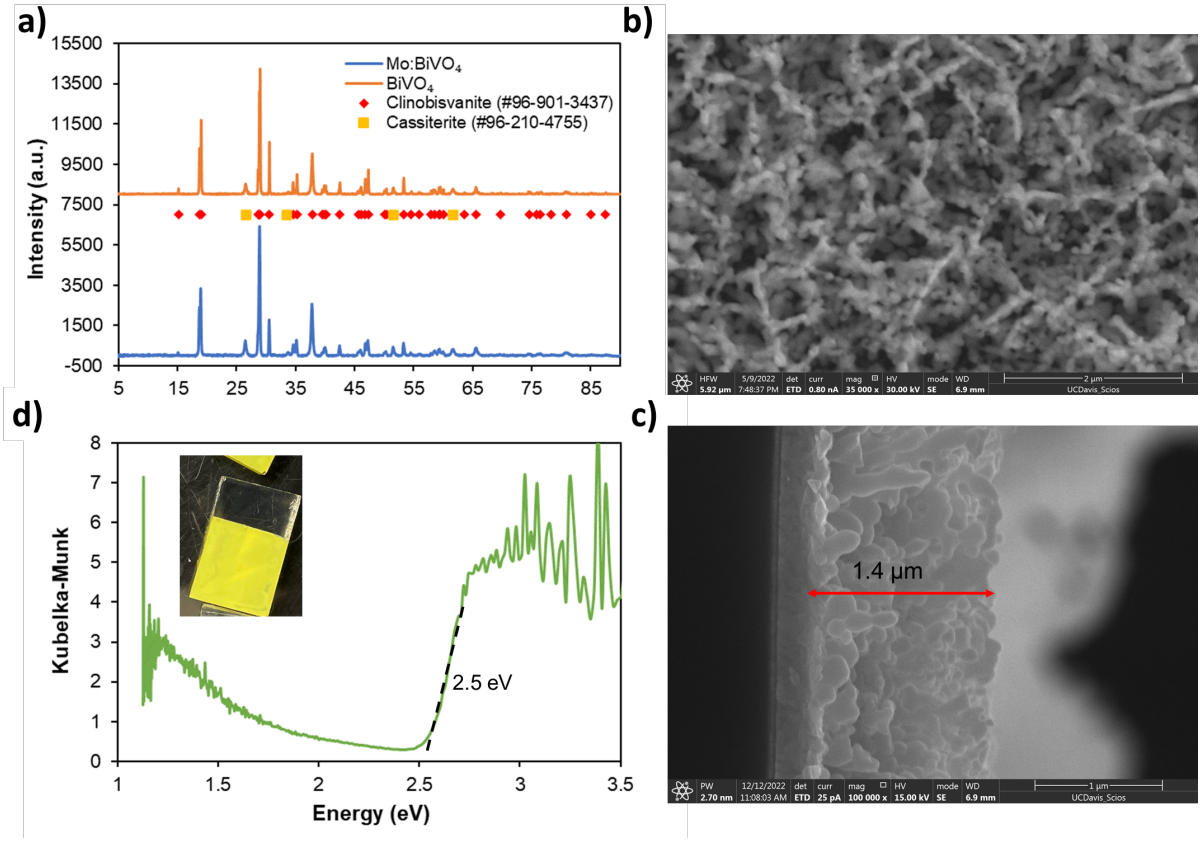

Figure 1. a) Powder XRD patterns for $BiVO_4$ and Mo:$BiVO_4$ on FTO (Cu-K_α radiation, 1.5418 Å) and reference pattern. b) Scanning Electron Micrographs of $BiVO_4$ film on FTO and c) cross-section. The morphology of the film is similar to the previous report. [22] d) Diffuse Reflectance Kubelka Munk plot for FTO/$BiVO_4$. Photo of film in insert.

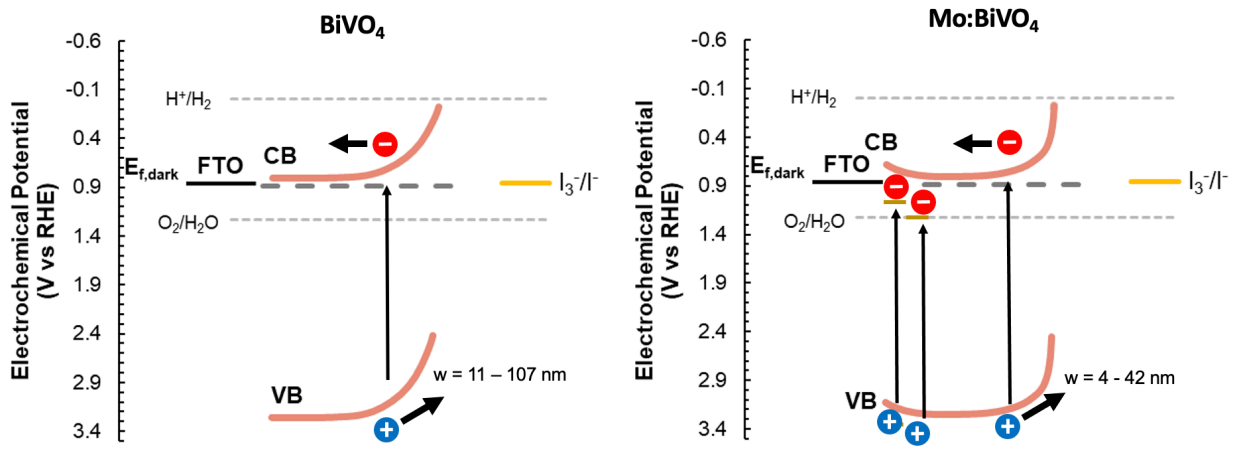

Figure 2. Energy diagrams for FTO/$BiVO_4$/(I_3^-/I^-) and FTO/Mo:$BiVO_4$/(I_3^-/I^-) junctions in the dark (5 mM I_3^- /0.1 M I^- in 0.05M PBS at pH 6.66). The space charge layer thickness (*w*) range for each electrode was calculated with the Poisson equation using literature and experimental data in **Table S5**. [24]

Based on its flatband potential of 0.1 V RHE (**Table S5**), $BiVO_4$ is expected to form a junction in contact with a triiodide/iodide solution (**Figure 2**). Because Mo-doping raises the free electron density in $BiVO_4$, its flatband potential is slightly more negative (0.05 V RHE). [25] This increases the built-in voltage of the Mo-doped $BiVO_4$ film relative to the non-doped $BiVO_4$ film but makes its depletion layer width ~60% smaller, depending on the estimated donor density in **Table S5**. Under illumination, each junction is expected to move electrons to the back contact and photoholes to the electrolyte, causing iodide oxidation. This can be verified with photoelectrochemical scans (**Figure 3**) of the films in phosphate buffered I_3^-/I^- (5.0 mM / 0.10 M) electrolyte (pH 6.66) under chopped 470 nm LED illumination (193 mW cm^{-2}). At potentials negative of 0.3 V RHE a cathodic dark current appears that can be attributed to I_3^- reduction, while above 0.30 V RHE, an anodic

photocurrent forms that is due to iodide oxidation. The anodic photocurrent reaches 0.59 mA - 0.75 mA at 0.85 V vs RHE (the iodide oxidation potential) for the $BiVO_4$ and Mo:$BiVO_4$ electrodes, respectively (**Figure 3a,b**). Mo-doping shifts the anodic photocurrent onset potential of the $BiVO_4$ film from 0.30 V RHE to 0.34 V RHE. Overall, these onsets are about 100 mV negative of the reported onset potential for water oxidation (0.44 V RHE).[22] This is the result of the faster charge transfer reaction with iodide and its more reducing standard potential. As will be shown below, the anodic photocurrents are entirely due to iodide oxidation and water oxidation is not a side reaction.

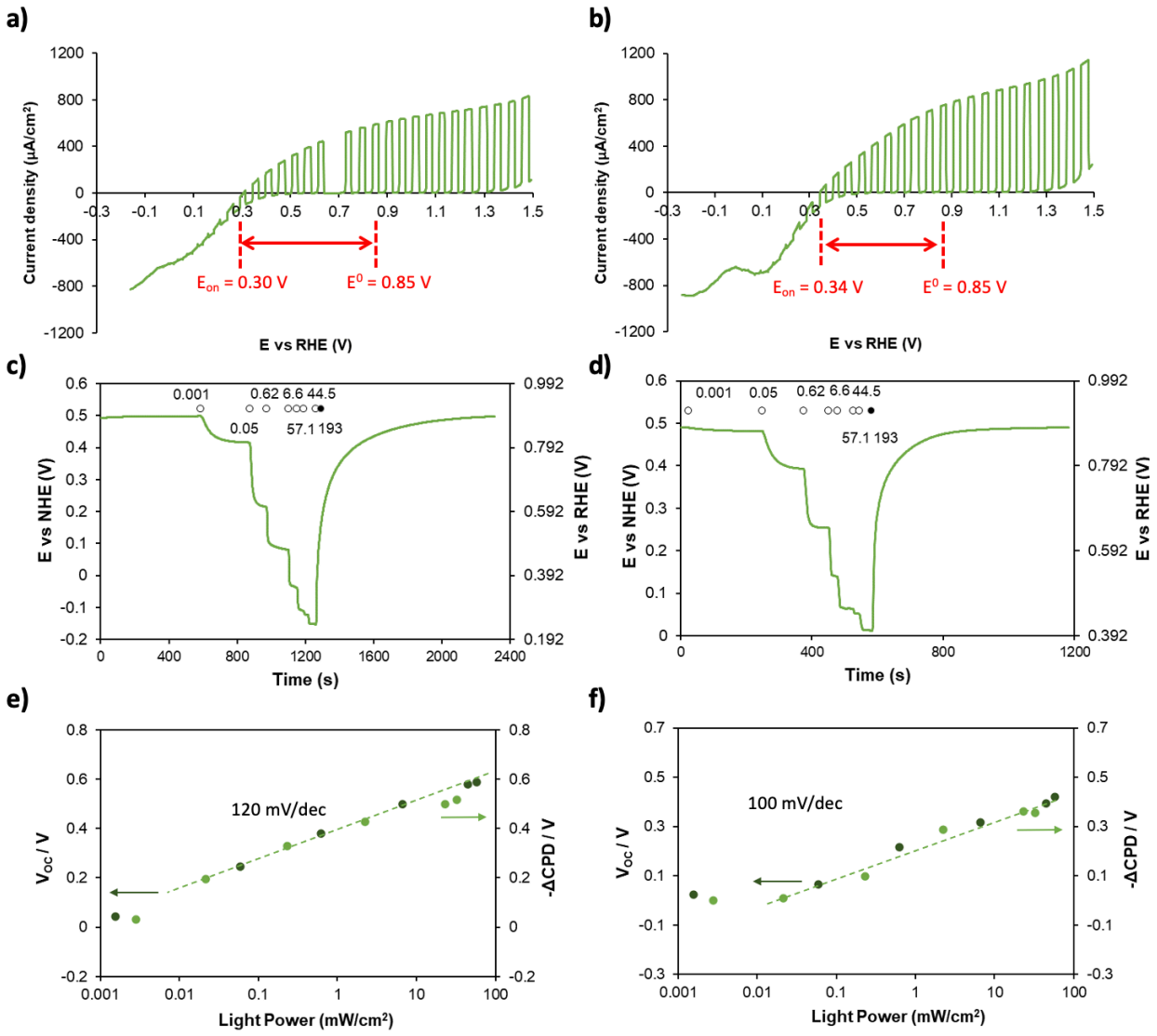

Figure 3. Photoelectrochemical data for $BiVO_4/(I_3^-/I^-)$ (a, c, e) and for $Mo:BiVO_4/(I_3^-/I^-)$ junctions (b, d, f). a - b) Chopped light linear sweep voltammograms (470 nm LED, 193 mW cm^{-2}; scan direction from right to left), c - d) Open circuit potential measurements, and e – f) plots of SPV and V_{OC} versus logarithm of light intensity in N_2-purged electrolyte I_3^-/I^- (50 mM/1.0 M in 50 mM PBS at pH 6.66) electrolyte. White and dark circles indicate light and dark periods and numerical values indicate irradiance (mW cm^{-2}).

Based on the PEC data, the photovoltage of the $BiVO_4$ electrode is 0.55 V (0.85 V – 0.30 V) and that of Mo:$BiVO_4$ electrode 0.50 V (both under 193 mW cm^{-2} illumination from a 470 nm LED). To determine the photovoltage of the photoelectrodes under variable illumination conditions, open circuit potential measurements were conducted using a saturated calomel counter-electrode **(Figure 3c,d)**. The open circuit potential provides the electrochemical potential $E_{F,b}$ at the $BiVO_4$ back contact relative to the standard reduction potential of the solution E^0 (**equation 1**).

$$V_{OC} = E_{F,b} - E^0 \qquad (1)$$

In the dark, both non-doped $BiVO_4$ and Mo-doped films have nearly identical $E_{F,b}$ values of 0.891 V and 0.886 V vs RHE. These values are close to the calculated redox potential of the 0.0050/ 0.10 M KI_3/KI electrolyte at pH 6.66 (E^0=0.853 V RHE). This shows that the electrodes are in electrochemical equilibrium with the triiodide/iodide couples. Increasing illumination intensity moves the $E_{F,b}$ values to more negative potential, as expected for a photoanode. Plots of the V_{OC} values versus the log of the light intensity are shown in **Figure 3e and f**. Graphs are linear, as expected from the Shockley diode equation, [26-28] with some deviations at low intensity, due to incomplete illumination of the junction. From the slopes (119 mV dec^{-1} for the $BiVO_4$ and 92 mV dec^{-1} for the Mo doped film), the diode ideality factors, γ can be calculated as 2.0 and 1.5. The deviation from unity is not unexpected for photoelectrochemical cells, where trapping of charge carriers at the solid-liquid interface is frequent, leading to changes in band bending and barrier heights.[29-30]

Based on its 2.4 eV bandgap, $BiVO_4$ absorbs 15% of the photons of AM 1.5 light (5.5 x 10^{20}

photons s^{-1} m^2), which corresponds to 23 mW cm^{-2} of 470 nm light from an LED. Therefore, V_{OC} under AM 1.5 illumination can be estimated from the open circuit voltage under 23 mW cm^{-2} 470 nm illumination. This yields values for V_{OC} = 0.36 V for Mo:$BiVO_4$ and V_{OC} = 0.55 V for $BiVO_4$ (**Fig. 3e,f**). The lower photovoltage value for Mo:$BiVO_4$ was also seen in the PEC scans. It is attributed to increased recombination resulting from Mo defects, as is typical for electron donor dopants, such as tungsten. [6, 31] Overall, the PEC and V_{OC} data suggests that the combination of a FTO/$BiVO_4$ photoelectrode with a I_3^-/I^- electrolyte can produce a solar cell. To test this idea, sandwich devices employing FTO/$BiVO_4$ and FTO/Mo:$BiVO_4$ photoelectrodes were constructed as shown in **Figure 4**. First, a Pt counter electrode was fabricated on FTO and contacted with a strip of indium metal. The electrode was then sandwiched against the FTO/$BiVO_4$ working electrode using a 25 μm spacer, after which the volume between the two electrodes was filled with a phosphate buffered KI_3/KI (0.005/ 0.10 M) electrolyte (pH 6.66).

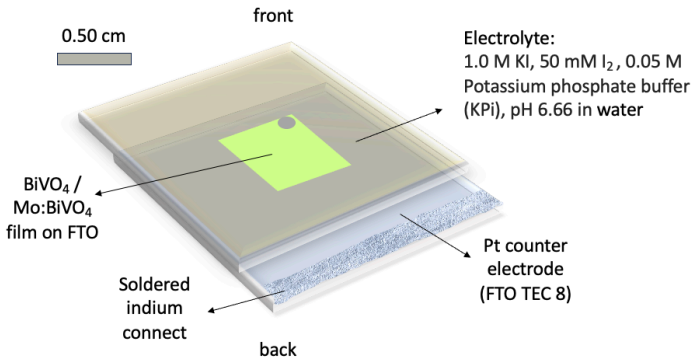

Figure 4. Schematic view of the sandwich solar cell. Illumination occurs through the $BiVO_4$ coated FTO front side.

Representative *J-V* curves in the dark and under AM 1.5 illumination for the two sandwich devices are shown in **Figure 5a** and performance data averaged over 6 devices is summarized in **Table S8**. Cells convert solar energy into electricity with efficiencies of 0.14% for the Mo:$BiVO_4$ device and 0.17% for the $BiVO_4$ device. A slightly higher efficiency of 0.22 % is seen for a thinner $BiVO_4$

film (**Table S8**). Open circuit potentials average at -0.32 ± 0.15 V for the $BiVO_4$ devices and -0.25 ± 0.03 V for the Mo:$BiVO_4$ device. The lower open circuit voltage of Mo:$BiVO_4$ agrees with the PEC data in **Figures 3** and is due to increase electron/hole recombination. At the same time, the Mo:$BiVO_4$ devices have larger short circuit photocurrents (1.8 ± 0.17 mA cm^{-2}) than the $BiVO_4$ devices (1.46 ± 0.17 mA cm^{-2}). This is a result of the higher conductivity resulting from the increased electron concentration after Mo-doping (**Table S5**). The linear *J-V* response near short circuit (**Figure 5a,b**) suggests that shunting is significant. This is not surprising given the porosity of the $BiVO_4$ films **(Figure S4)**, which do not fully prevent direct contact between the underlying FTO substrate and the I_3^-/I^- electrolyte. The *J-V* curves can be fit to the modified diode equation which includes the shunt resistance, R_{shunt}:

$$J = J_{photo} - J_0\, e^{qv/\gamma kT} - V/R_{shunt} \qquad (2)$$

where J_0 is the exchange (recombination) current density, q is the charge of an electron, k is the Boltzmann constant and T is temperature. The fitted J-V curves nicely describe the behavior with a shunt resistance and diode quality factors between 3 and 4 (γ in **Table S9**). The larger diode quality factor and the smaller shunt resistance are consistent with the lower fill factor of the Mo-doped $BiVO_4$ film. Diode quality factors from the J-V curves are higher than the values from the SPV data in **Figure 3e/f**. This might be due to the different illumination conditions during these experiments (front illumination for the J-V experiment and back illumination for the SPV experiment). Also, while SPV measurements were performed without applied bias, J-V curves were obtained under forward bias, which leads to decreased band bending and better conductivity of the $BiVO_4$ liquid junction.

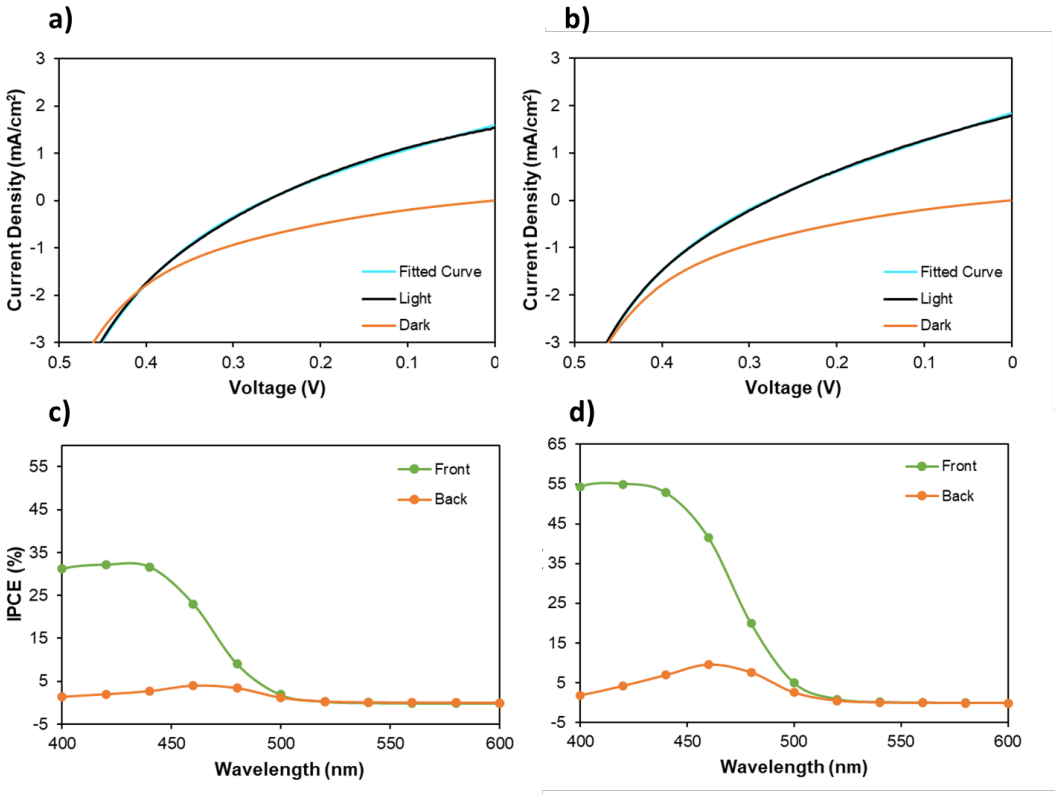

Figure 5. Performance Data for left: $BiVO_4/(I_3^-/I^-)$ and right: $Mo:BiVO_4/(I_3^-/I^-)$ solar cells (50 mM I_3^- /1 M I^- in 50 mM PBS at pH 6.66). a) ,b) *J-V* curves measured in the dark (orange) and under AM1.5 illumination (green), as well as fitted curve (cyan), c), d) IPCE spectra measured in response to front side (black) and back side (red) illumination.

The photoaction spectra in **Figure 5c,d** correlate well with the optical absorption of $BiVO_4$. Front (substrate side) illumination provides a substantially higher Incident Photon-to-Current Efficiency (IPCE) value than back illumination through the electrolyte. This is primarily a result of shading from the Pt counter electrode and from the I_3^-/I^- electrolyte. It is known that platinum counter electrodes account for approximately 10 % uniform loss in transmittance. [32] Even with in thin layer sandwich cell containing a diluted solution of 50 mM I_3^-, the strong absorption of the triiodide ion (ε = 4.44 mM^{-1} cm^{-1} at 400 nm) results in ~70% loss of transmitted light at 400 nm (**Figure S6**).

Slow electron diffusion in $BiVO_4$ accounts for the remaining difference in performance under back versus front illumination. [33] Electron transport is improved in the Mo:$BiVO_4$ device, allowing a higher IPCE of 41% compared to 23% for the $BiVO_4$ device at 470 nm. As **Figure S7** shows, the integrated IPCE agrees with the measured short circuit current densities in the I-V curves.

To better understand the factors that limit the photovoltage of the $BiVO_4$ solar cells, vibrating Kelvin probe Surface Photovoltage (SPV) spectra were recorded on the $BiVO_4$ photoanodes in contact with the electrolyte. The measurement configuration is shown in **Figure S10**. We previously showed that the SPV signal generated under these conditions equals the photovoltage V_{ph} of the illuminated FTO/$BiVO_4$ electrode, [34-35] i.e. the difference of the electrochemical potentials at the front ($E_{F,f}$) and back ($E_{F,b}$). SPV spectra for a $BiVO_4$ photoelectrode in contact with triiodide/iodide electrolyte are depicted in **Figure 6a**. A negative SPV signal is generated at photon energies above 2.35 eV, close to the optical bandgap of $BiVO_4$. This confirms that the SPV signal results from charge separation in the $BiVO_4$ depletion layer, as expected from **Figure 3**. The signal reaches its maximum of - 435 mV at 470 nm in the 5.0 mM I_3^- /0.10 M I^- electrolyte, and then drops off at higher photon energy, due to incomplete illumination of the film. This is a result of the low light intensity during the SPV measurements (0.64 mW cm^{-2} at 470 nm) and the decreasing light penetration depth with higher photon energy. The spectrum in the 50 mM I_3^- /1.0 M I^- electrolyte is similar, except the photovoltage is smaller (-391 mV at 470 nm), which is a result of shading from the triiodide ion at wavelengths below 480 nm (**Figure S6**).

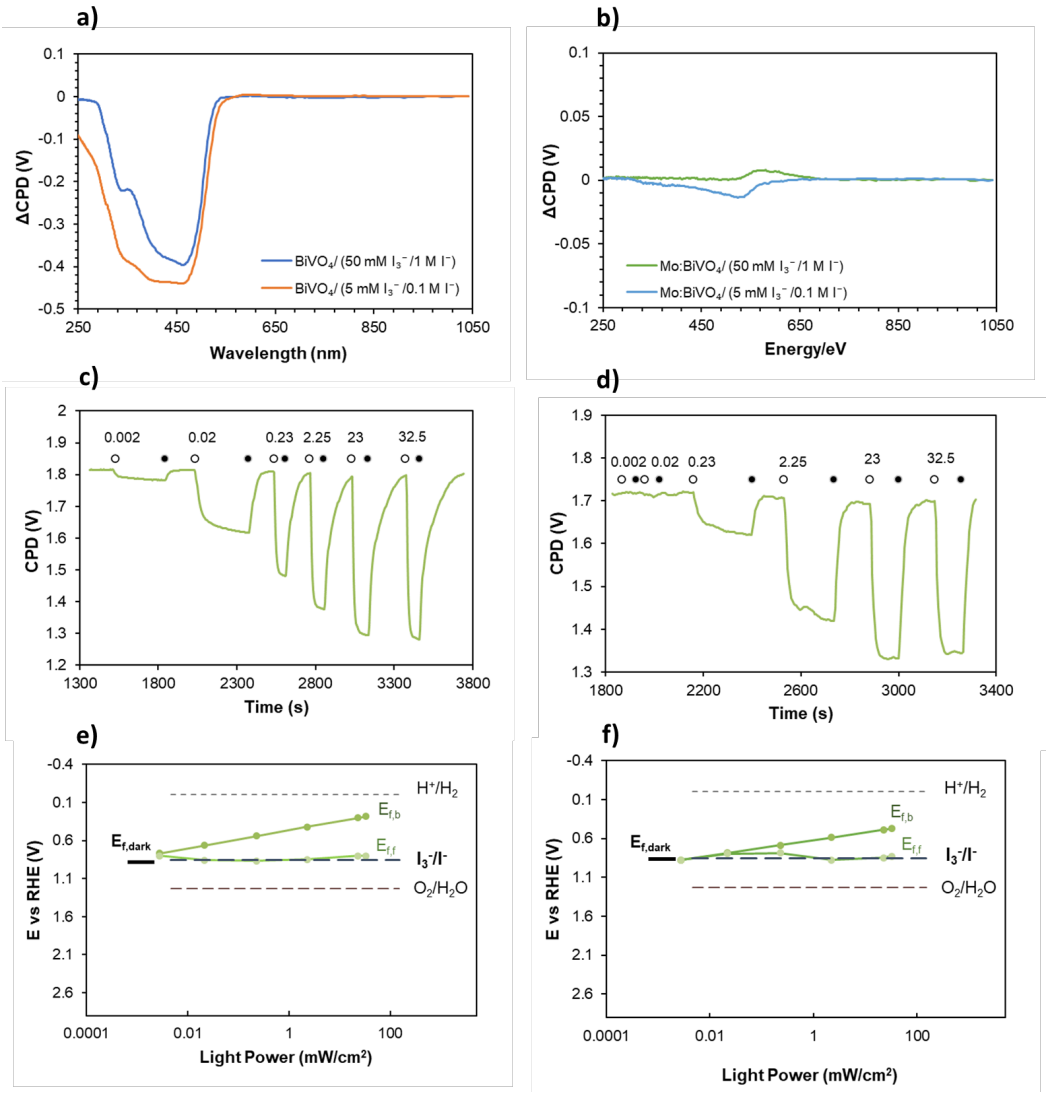

Figure 6. a) SPV spectra of $BiVO_4$ and b) Mo:$BiVO_4$ in contact with 50 mM I_3^- / 1.0 M I^- in 50 mM PBS at pH 6.66 and 5.0 mM I_3^- /0.10 M I^- in 50 mM PBS at pH 6.66. The scan direction is from low to high energy. c) SPV of $BiVO_4$ and d) Mo:$BiVO_4$ under intermittent illumination from a 470 nm LED. Fermi levels in e) $BiVO_4$/(I_3^-/I^-) and f) Mo:$BiVO_4$/(I_3^-/I^-) junctions versus irradiance (470 nm).

SPV spectra for the Mo:$BiVO_4$ photoelectrode are shown in **Figure 6b**. The SPV signal is much smaller, or even inverted to positive voltage when a more concentrated I_3^-/I^- electrolyte is used.

The smaller negative SPV signal suggests that charge separation in the Mo:$BiVO_4$ is weakened as a result of the higher electron hole recombination rate resulting from the Mo dopant. The positive (inverted) SPV signal is seen with the higher iodide electrolyte concentration. It occurs at 570 nm, just below the $BiVO_4$ band gap, where the light can penetrate the entire Mo:$BiVO_4$ film and reach the FTO interface. Similar inverted SPV signals were observed previously for CdSe quantum dots, [36] in GaAs and $SrTiO_3$ films, [37] and in GaN nanowire arrays. [38] They indicate a detrimental junction at the FTO/Mo:$BiVO_4$ contact (see **Figure 2b**). This junction creates a barrier for electron injection into FTO which reduces the photoanode performance of the Mo:$BiVO_4$ film. No junction is observed for the FTO/$BiVO_4$ configuration because the lower Fermi level of $BiVO_4$ (0.10 V vs RHE) compared to Mo:$BiVO_4$ (0.05 V RHE) favors an Ohmic contact with FTO.

Next, to correlate the SPV signal with the illumination intensity, SPV signals were recorded under intermittent 470 nm illumination (**Figure 6c and d**). As before, the photovoltage signals are negative. Transient photovoltage signals form quickly (15 s under 23 mW cm^{-2} illumination) and decay more slowly (61 s) after the light is turned off. Slower timescales for the SPV signal decay are frequently observed in transient surface photovoltage data for semiconductor films. [38-41] We attribute this to several factors, including a decreased charge carrier concentration in the dark, a change in the charge carrier transport mechanism from *drift* under illumination to *diffusion* in the dark, and to trapping of minority carriers in deep surface states. The transient SPV data for the Mo:$BiVO_4$ film is shown in **Figure 6d**. As before in **Figure 5b**, no photovoltage is observed for the two lowest light intensities (0.002 and 0.02 mW/cm^2). At 23 mW cm^{-2} under 470 nm, signals form on the 15 s time scale and decay on the 20 s timescale. The much faster decay compared to the $BiVO_4$ film is attributed to improved electron transport in the material and to an increased

electron-hole recombination rate at the Mo sites. The photovoltages at 23 mW cm^{-2} under 470 nm illumination are 0.36 V for Mo:$BiVO_4$ and 0.51 V for $BiVO_4$ (**Fig. 6c,d**), which is comparable to the open circuit potential measurements.

Figure 3e and f plot the SPV data together with the open circuit potential V_{OC} as a function of light intensity. For both electrodes the SPV signals closely approach the V_{OC}. This is expected from the theory for a photoelectrochemical cell with a fast redox couple. Here, $V_{Ph} = V_{OC}$ and from SPV = V_{ph}, as shown in our previous work.[35] Using $V_{ph} = E_{F,f} - E_{F,b}$, the minority carrier electrochemical potential at the electrode/liquid contact $E_{F,f}$ can now be calculated for all illumination conditions. This data is shown for the FTO/$BiVO_4$ electrode in **Figures 6e**. In the dark, only one common Fermi level $E_{F,b}$ is seen, which equals the electrochemical potential of the electrolyte E^0. Under illumination, $E_{F,b}$ and $E_{F,f}$ split into two levels, whose difference corresponds to the photovoltage. It can be seen that $E_{F,b}$ becomes more reducing with increasing light intensity, while $E_{F,f}$ remains close to E^0. This 'Fermi level equilibration' is a result of the fast charge transfer kinetics between $BiVO_4$ and the redox couple. This shows that the $BiVO_4$ surface is natively electrocatalytic for iodide oxidation. Furthermore, the value of $E_{F,f}$ rules out the possibility of water oxidation under these conditions, which requires $E_{F,f}$ of 1.23 V RHE or greater. Photovoltage values for the Mo:$BiVO_4$ photoelectrode (**Figure 6f**) lag behind values seen for the $BiVO_4$ electrode, with no photovoltage seen at the two lowest light intensities. This is attributed to electron hole-recombination at molybdenum defects, and to reduced electron transfer across the detrimental junction at the FTO/Mo:$BiVO_4$ interface (**Figure 2b**). Overall, the Fermi Level plots in **Figure 6e,f** reveal that the photovoltage of both $BiVO_4$/(I_3^-/I^-) solar cells are fundamentally limited by the triiodide/iodide redox potential, which pins the $E_{F,f}$ levels. Higher photovoltages

should be possible by using a more oxidizing redox couple, such as $IrCl_6^{2-/3-}$ (E^0= 0.87 V vs NHE). One can also imagine a $BiVO_4$ regenerative cell employing the O_2/H_2O (E^0= 1.23 V vs NHE) redox couple, in analogy to the photogalvanic TiO_2 devices mentioned in the introduction.

Conclusion

In summary, we provide the first example of a $BiVO_4$ photovoltaic cell. The 0.5 x 0.5 cm^2 devices employ a solid-liquid junction with an aqueous triiodide/iodide redox couple. The champion device reaches an energy conversion efficiency of 0.22 %, photovoltage of 0.36 V and a photocurrent of 1.58 mA cm^{-2} under AM 1.5 illumination. The performance is much below that of conventional dye sensitized solar cells, whose dye's absorption is matched to the solar spectrum.[42-44] In contrast, $BiVO_4$ with its 2.4 eV band gap permits absorption of only 12% of the solar flux, and is limited by electron-hole recombination, as verified by IPCE measurements under front and back illumination. Mo-doped films produce higher photocurrents, due to the higher donor concentration and conductivity, but lower photovoltage due to increased recombination at Mo defects. The main photovoltage loss of these devices is caused by the mismatch between the $BiVO_4$ valence band and the triiodide/iodide standard reduction potential. Additional photovoltage losses result from a detrimental junction at the FTO/Mo:$BiVO_4$ interface, as revealed by liquid SPV measurements and from back electron transfer to triiodide by the FTO substrate, based on modeling of the J-V data. Liquid SPV shows that the electrochemical potential of the minority carriers $E_{F,f}$ is pinned to the triiodide/iodide reduction potential over the entire illumination range. This rules out competing water oxidation under operating conditions. Theoretically, improved $BiVO_4$ devices with higher V_{OC} are possible by replacing the triiodide/iodide couple with a more

oxidizing redox couple [45] and by addressing the junction / back electron transfer problems at the FTO back contact. Overall, the work demonstrates the possibility of photovoltaic devices using metal oxide absorbers in contact with aqueous electrolytes. Even though the larger band gaps of metal oxides limit their solar energy conversion efficiency, the visible light transparency and the deep valence bands are attractive features for the construction of tandem photovoltaic devices in combination with main group element semiconductors.

Acknowledgement

FEO thanks the U.S. Department of Energy, Office of Science, Office of Basic Energy Sciences under Award Number DOE-SC0015329 for financial support of this work. TWH thanks Chemical Sciences, Geosciences, and Biosciences Division, Office of Basic Energy Sciences, Office of Science, the U.S. Department of Energy grant no. DE-SC0017342 for support of this research. We thank Peter Cendula (University of Žilina, Slovakia) for useful discussions.

Supporting Information

The following supporting information is available: Selected Semiconductor Data, [19, 22-23, 25, 33, 35, 46] Photos of the Photoelectrodes, Open Circuit Potential Data, Short Circuit Photocurrent Data, Surface photovoltage data, Optical Absorption spectrum, I-V current, Energy diagrams, Schematics and Tables.

Experimental

The chemicals used in the syntheses of the materials are Bismuth(III) nitrate pentahydrate (99.999

%, Acros Organics), Nitric acid (70.0 %, Sigma-Aldrich), Vanadyl acetylacetonate (99%; Acros Organics), Bis(acetylacetonato)dioxomolybdenum(VI) (95%; Strem Chemicals), Dimethyl sulfoxide (≥99.9%; Sigma-Aldrich), P-benzoquinone (≥98%; Sigma-Aldrich), Potassium iodide (99.0%; Merck), Iodine (≥99.8%; Sigma-Aldrich), Potassium phosphate monobasic (98%; Sigma-Aldrich,) and Potassium hydroxide (≥97%; Sigma-Aldrich), FTO (MTI Corp.,TEC 15, Resistance 12-14Ω, Thickness 2.2mm). Water for the syntheses and photocatalytic experiments was purified to 18 MΩ cm.

$BiVO_4$ film preparation

The FTO pieces of 1.0 cm^2 surface area were cleaned with soap solution by sonicating for 5 minutes, followed by sonication in methanol, ethanol, isopropanol, acetone (15 min each). . $BiVO_4$/ FTO was prepared using the published procedure. [22] In summary, 50 mL of a 0.40 M KI solution with pH of 1.7 (adjusted by adding 2.0 M HNO_3) was prepared, followed by dissolving 0.970 gr of $Bi(NO_3)_3 \cdot 5\ H_2O$ in 50 mL of a 0.4 M KI to prepare 0.040 M $Bi(NO_3)_3$ solution. This solution was then mixed with 20 mL of absolute ethanol containing 0.23 M p-benzoquinone. A typical three-electrode cell was used for electrodeposition containing the prepared solution with FTO as working electrode (WE), a Calomel (3.5 M KCl) as reference electrode (RE), and a platinum counter electrode (CE). BiOI electrodes were electrodeposited on FTO substrate for 3-5 min. In the next step, 0.10 mL of a dimethyl sulfoxide (DMSO) solution containing 0.20 M vanadyl acetylacetonate ($VO(acac)_2$) was drop-coated on the BiOI electrode, followed by calcination at 450 ^oC and then etching in 1.0 M NaOH for 30 min to remove excess V_2O_5. Digital photos of BiOI/FTO and $BiVO_4$/ FTO are shown in Figure S6. Mo-doped $BiVO_4$ was prepared by drop coating of $VO(acac)_2$ in DMSO containing 1 molar% $Mo(acac)_2$, followed by calcination at 450 C

and etching in 1.0 M NaOH for 30 min.

Sandwich Solar Cell Fabrication

Platinum Counter Electrode: Single holes were drilled on bare fluorine-doped tin oxide, FTO (TEC 8, Hartford). The FTO was cut into 1.5 cm x 1.0 cm pieces. The FTO pieces were cleaned with soap solution by sonicating for 5 minutes, followed by sonication in DI water (5 min). Next they were rinsed with 0.10 M HCl solution in ethanol and sonicated in acetone for 10 minutes. The FTO pieces were then heated for 15 minutes at 400°C. Platinum was deposited by coating a drop of 5.0 mM H_2PtCl_6 in isopropanol. The drop was tilted to spread, and dried for 5 minutes. The Pt coated FTO pieces were then heated to 380°C for 20 minutes and then cooled to room temperature.

Cell Assembly: The $BiVO_4$ photoanode and the Pt counter electrode were sandwiched together using 25 μm Surlyn films. They were placed on a 140°C hotplate and pressure was applied. The electrolyte was injected into the cell through the predrilled hole in the counter electrode and vacuum was pulled on it. The cell was then sealed with Suryln film and cover slip by melting the edges of the film with the help of a soldering iron. Electrical contact was applied to the cell with melted indium.

Electrolyte Preparation

The 1.0 M phosphate buffer stock solution (PBS) at pH 6.66 was prepared by dissolving 3.40 g KH_2PO_4 in 250 mL of water, followed by adjusting the pH to 6.66 with 2.0 M KOH solution. Then, 0.05 M PBS was prepared by diluting the stock solution appropriately. A pH of 6.66 was adjusted further with 2.0 M KOH solution using a pH meter (Fisher Scientific *Accumet* AE150). The triiodide/iodide solution was prepared using 1.0 M potassium iodide (KI), 50 mM iodine (I_2) and

0.050 M Potassium phosphate buffer (95%/5% molar ratio) in water. This was done by adding 1.66 g of KI and 0.128 g of I_2 to 0.050 M PBS. The pH was adjusted to 6.66 with the 2.0 M KOH solution. The $E^{0'}$ was calculated as follows: $E^{0'} = E^0$ (NHE) + 0.059 V x pH - 0.059 V x log (Ox/Red) = 0.536 V + 0.059 V x (6.66) + 0.059 V x log (0.05/0.95) = 0.853 V (RHE).

Measurements

For electrochemical measurements, a Gamry Reference 600 Potentiostat was used together with a three-electrode cell, where the FTO/$BiVO_4$ electrodes served as working electrodes and Pt as a counter electrode. A 3.5 M KCl calomel reference electrode was connected to the cell via a 3.5 M KCl salt bridge. Cyclic voltammetry scans were recorded at 10 mV/s from positive to negative potentials. The cell was degassed for 20 mins with nitrogen prior to measurements. A monochromatic LED (470 nm) with a fixed light intensity was used for photocurrent measurement. For open circuit potential (OCP) measurements a two-electrode system consisting of the FTO/$BiVO_4$ working electrode and a 3.5 M KCl calomel reference electrode with a KCl saltbridge was used. The light intensity was changed from the lowest to highest values. The system was calibrated using a cyclic voltammetry scan in 1:1 molar $K_4[Fe(CN)_6]$/ $K_4[Fe(CN)_6]$ electrolyte using the published standard reduction potential of +0.358 V (NHE). Measured potentials (NHE) were then converted to the Relative Hydrogen Electrode scale using $E_{RHE}=E_{NHE}$ + 0.059 V x pH.

Solar cell measurements were conducted with an Autolab PGSTAT 128N potentiostat with a xenon arc lamp. Sunlight simulation at 100 mW cm^{-1} was obtained using an AM 1.5 solar filter. An Oriel Reference Solar Cell and Meter were used to calibrate the light intensity. A Horiba Jobin Yyon MicroHR monochromator with a 450 W xenon arc lamp was used for IPCE measurements.

A Nova II Ophir power meter was used to measure the photon flux of incident light on cells. A mask with an area of 0.16 cm^{-2} was applied on top of the active area of the cells.

UV-visible diffuse reflectance spectroscopy (DRS) was performed with a Thermo Scientific Evolution 220 spectrometer, equipped with an integrating sphere and using a $BaSO_4$ as the reference. The reflectance data were converted to the Kubelka−Munk function. The optical bandgap was estimated by using the Kubelka–Munk conversion and applying the tangential method.

Surface photovoltage (SPV) measurements were conducted under N_2 wet gas environment using a vibrating gold Kelvin probe (Delta PHI Besocke). Samples were illuminated with monochromatic light from a 150 W Xe lamp filtered through an Oriel Cornerstone 130 monochromator (~1 mW cm^{-2}). The signal drift in the full spectra was corrected by subtracting a dark background from the raw data. All reported contact potential difference (CPD) values are referenced relative to the CPD value in the dark. Effective bandgaps were obtained from the major photovoltage signals in the spectra using the tangent method.

Powder X-ray diffraction scans were performed using a Bruker D8 Advance Eco with a Cu Kα and a monochromatic wavelength of 1.5418 Å. Scanning electron microscopy (SEM) images were recorded using FEI Scios equipment at operating voltages of 5 kV for SEM images. Elemental analysis of sample was done using Oxford X-Max Energy Dispersive X-ray Spectroscopy (EDS) Detector at 20 keV.

For the SPV measurements in aqueous medium, 20 μL of aqueous solution was dropped onto the surface of film followed by mounting a microscope glass on the drop. The sample was then

mounted inside of a custom made chamber which was filled with water vapor saturated N_2 gas. Gas flow was continued throughout the measurement at a flow rate of 0.03 L/min.

For all transient SPV measurements 1.0 M KI / 0.05 M I_2 in 0.050 M PBS was used as electrolyte. For photoelectrochemistry measurements, a diluted solution (0.10 M KI / 5.0 mM I_2) was utilized to reduce light shading. The 0.10 M KI/ 5.0 mM I_2 solution was prepared by adding 0.166 g of KI and 0.0128 g of I_2 to 0.050 M PBS.

References

1. Park, Y.; McDonald, K. J.; Choi, K. S., Progress in Bismuth Vanadate Photoanodes for Use in Solar Water Oxidation. *Chem. Soc. Rev.* **2013,** *42* (6), 2321-2337.

2. Kim, J. H.; Lee, J. S., Elaborately Modified BiVO4 Photoanodes for Solar Water Splitting. *Adv. Mater.* **2019,** *31* (20), 1806938.

3. Kudo, A.; Ueda, K.; Kato, H.; Mikami, I., Photocatalytic O-2 Evolution under Visible Light Irradiation on BiVO4 in Aqueous AgNO3 Solution. *Catalysis Letters* **1998,** *53* (3-4), 229-230.

4. Liang, Y. Q.; Tsubota, T.; Mooij, L. P. A.; van de Krol, R., Highly Improved Quantum Efficiencies for Thin Film BiVO4 Photoanodes. *J. Phys. Chem. C* **2011,** *115* (35), 17594-17598.

5. Kato, H.; Hori, M.; Konta, R.; Shimodaira, Y.; Kudo, A., Construction of Z-scheme type heterogeneous photocatalysis systems for water splitting into H-2 and O-2 under visible light irradiation. *Chemistry Letters* **2004,** *33* (10), 1348-1349.

6. Nair, V.; Perkins, C. L.; Lin, Q.; Law, M., Textured nanoporous Mo:BiVO4 photoanodes with high charge transport and charge transfer quantum efficiencies for oxygen evolution. *Energ. & Environ. Sci.* **2016,** *9* (4), 1412-1429.

7. Walsh, A.; Yan, Y.; Huda, M. N.; Al-Jassim, M. M.; Wei, S.-H., Band Edge Electronic Structure of BiVO4: Elucidating the Role of the Bi s and V d Orbitals. *Chemistry of Materials* **2009,** *21* (3), 547-551.

8. Bhatt, M. D.; Lee, J. S., Recent theoretical progress in the development of photoanode materials for solar water splitting photoelectrochemical cells. *J. Mater. Chem. A* **2015,** *3* (20), 10632-10659.

9. Long, M.; Cai, W. M.; Cai, J.; Zhou, B. X.; Chai, X. Y.; Wu, Y. H., Efficient photocatalytic degradation of phenol over Co3O4/BiVO4 composite under visible light irradiation. *J. Phys. Chem. B* **2006,** *110* (41), 20211-20216.

10. Seabold, J. A.; Choi, K. S., Efficient and Stable Photo-Oxidation of Water by a Bismuth Vanadate Photoanode Coupled with an Iron Oxyhydroxide Oxygen Evolution Catalyst. *Journal of the American Chemical Society* **2012,** *134* (4), 2186-2192.

11. Park, H. S.; Leonard, K. C.; Bard, A. J., Surface Interrogation Scanning Electrochemical Microscopy (SI-SECM) of Photoelectrochemistry at a W/Mo-BiVO4 Semiconductor Electrode: Quantification of Hydroxyl Radicals during Water Oxidation. *J. Phys. Chem. C* **2013,** *117* (23), 12093-12102.

12. Zhong, D. K.; Choi, S.; Gamelin, D. R., Near-Complete Suppression of Surface Recombination in Solar Photoelectrolysis by "Co-Pi" Catalyst-Modified W:BiVO4. *Journal of the American Chemical Society* **2011,** *133* (45), 18370-18377.

13. Zhang, B.; Zhang, X.; Xiao, X.; Shen, Y., Photoelectrochemical Water Splitting System—A Study of Interfacial Charge Transfer with Scanning Electrochemical Microscopy. *ACS Appl. Mater. Interfaces* **2016,** *8* (3), 1606-1614.

14. Qi, Y.; Zhao, Y.; Gao, Y.; Li, D.; Li, Z.; Zhang, F.; Li, C., Redox-Based Visible-Light-Driven Z-Scheme Overall Water Splitting with Apparent Quantum Efficiency Exceeding 10%. *Joule* **2018,** *2* (11), 2393-2402.

15. Abe, R.; Sayama, K.; Sugihara, H., Development of new photocatalytic water splitting into H-2 and O-2 using two different semiconductor photocatalysts and a shuttle redox mediator IO3 (-)/I-. *J. Phys. Chem. B* **2005,** *109* (33), 16052-16061.

16. Sasaki, Y.; Iwase, A.; Kato, H.; Kudo, A., The effect of co-catalyst for Z-scheme photocatalysis systems with an Fe3+/Fe2+ electron mediator on overall water splitting under visible light irradiation. *Journal of Catalysis* **2008,** *259* (1), 133-137.

17. Hamann, T. W., The end of iodide? Cobalt complex redox shuttles in DSSCs. *Dalton Transactions* **2012,** *41* (11), 3111-3115.

18. Long, M. C.; Cai, W. M.; Kisch, H., Visible light induced photoelectrochemical properties of n-BiVO4 and n-BiVO4/p-CO3O4. *J. Phys. Chem. C* **2008,** *112* (2), 548-554.

19. Vanysek, P., Electrochemical Series. In *CRC Handbook of Chemistry and Physics*, 88 (Internet Version 2008) ed.; CRC Press/Taylor and Francis: Boca Raton, FL, 2008.

20. Mavroides, J. G.; Tchernev, D. I.; Kafalas, J. A.; Kolesar, D. F., Photoelectrolysis of water in cells with TiO2 anodes. *Mater. Res. Bull.* **1975,** *10* (10), 1023-1030.

21. Laser, D.; Bard, A. J., SEMICONDUCTOR ELECTRODES .6. PHOTOELECTROCHEMICAL SOLAR-CELL EMPLOYING A TIO2 ANODE AND OXYGEN CATHODE. *Journal of the Electrochemical Society* **1976,** *123* (7), 1027-1030.

22. Kim, T. W.; Choi, K.-S., Nanoporous BiVO4 Photoanodes with Dual-Layer Oxygen Evolution Catalysts for Solar Water Splitting. *Science* **2014,** *343* (6174), 990-994.

23. Kudo, A.; Omori, K.; Kato, H., A novel aqueous process for preparation of crystal form-controlled and highly crystalline BiVO4 powder from layered vanadates at room temperature and its photocatalytic and photophysical properties. *Journal of the American Chemical Society* **1999,** *121* (49), 11459-11467.

24. Krol, R., Principles of Photoelectrochemical Cells. *Photoelectrochemical Hydrogen Production* **2012,** *102*, 13-67.

25. Rettie, A. J. E.; Lee, H. C.; Marshall, L. G.; Lin, J.-F.; Capan, C.; Lindemuth, J.; McCloy, J. S.; Zhou, J.; Bard, A. J.; Mullins, C. B., Combined Charge Carrier Transport and Photoelectrochemical Characterization of BiVO4 Single Crystals: Intrinsic Behavior of a Complex Metal Oxide. *Journal of the American Chemical Society* **2013,** *135* (30), 11389-11396.

26. Tan, M. X.; Laibinis, P. E.; Nguyen, S. T.; Kesselman, J. M.; Stanton, C. E.; Lewis, N. S., Principles and applications of semiconductor photoelectrochemistry. *Progress in Inorganic Chemistry, Vol 41* **1994,** *41*, 21-144.

27. Memming, R., Photoinduced Charge-Transfer Processes at Semiconductor Electrodes and Particles. In *Electron Transfer I*, 1994; Vol. 169, pp 105-181.

28. Salvador, P., Semiconductors' Photoelectrochemistry: A Kinetic and Thermodynamic Analysis in the Light of Equilibrium and Nonequilibrium Models. *J. Phys. Chem. B* **2001,** *105* (26), 6128-6141.

29. Aspnes, D. E.; Heller, A., Photoelectrochemical hydrogen evolution and water photolyzing semiconductor suspensions: properties of platinum group metal catalyst-semiconductor contacts in air and in hydrogen. *J. Phys. Chem. C.* **1983,** *87* (24), 4919-4929.

30. Lin, F. D.; Boettcher, S. W., Adaptive semiconductor/electrocatalyst junctions in water-splitting photoanodes. *Nature Mater.* **2014,** *13* (1), 81-86.

31. Abdi, F. F.; Savenije, T. J.; May, M. M.; Dam, B.; van de Krol, R., The Origin of Slow Carrier Transport in BiVO4 Thin Film Photoanodes: A Time-Resolved Microwave Conductivity Study. *J. Phys. Chem. Lett.* **2013,** *4* (16), 2752-2757.

32. Xie, Y.; Baillargeon, J.; Hamann, T. W., Kinetics of Regeneration and Recombination Reactions in Dye-Sensitized Solar Cells Employing Cobalt Redox Shuttles. *The Journal of Physical Chemistry C* **2015,** *119* (50), 28155-28166.

33. Abdi, F. F.; Firet, N.; van de Krol, R., Efficient BiVO4 Thin Film Photoanodes Modified with Cobalt Phosphate Catalyst and W-doping. *Chemcatchem* **2013,** *5* (2), 490-496.

34. Cheng, Y.; Xiao, C.; Mahmoudi, B.; Scheer, R.; Maijenburg, A. W.; Osterloh, F. E., Effect of charge selective contacts on the quasi Fermi level splitting of CuGa3Se5 thin film photocathodes for hydrogen evolution and methylviologen reduction. *EES Catalysis* **2023,** *1*, 74-83.

35. Daemi, S.; Kundmann, A.; Cendula, P.; Becker, K.; Osterloh, F. E., Contactless Measurement of Photovoltage in BiVO4 Photoelectrodes. *Energy Environ. Sci.* **2023,** *https://doi.org/10.1039/D3EE02087H*.

36. Zhao, J.; Nail, B. A.; Holmes, M. A.; Osterloh, F. E., Use of Surface Photovoltage Spectroscopy to Measure Built-in Voltage, Space Charge Layer Width, and Effective Band Gap in CdSe Quantum Dot Films. *J. Phys. Chem. Lett.* **2016**, 3335-3340.

37. Doughty, R. M.; Hodges, B.; Dominguez, J.; Han, R.; Zhao, Z.; Assavachin, S.; Osterloh, F. E., Fermi Level Pinning Controls Band Bending and Photochemical Charge Separation in Particles of n-SrTiO3, n-SrTiO3:Al, and n-GaAs:Te. *The Journal of Physical Chemistry C* **2020,** *124* (34), 18426-18435.

38. Doughty, R. M.; Chowdhury, F. A.; Mi, Z.; Osterloh, F. E., Surface photovoltage spectroscopy observes junctions and carrier separation in gallium nitride nanowire arrays for overall water-splitting. *The Journal of Chemical Physics* **2020,** *153* (14), 144707.

39. Han, R.; Kim, T.-Y.; Hamann, T. W.; Osterloh, F. E., Photochemical Charge Separation and Dye Self-Oxidation Control Performance of Fluorescein, Rose Bengal, and Triphenylamine Dye-Sensitized Solar Cells. *The Journal of Physical Chemistry C* **2020,** *124* (48), 26174-26183.

40. Roehrich, B. W.; Han, R.; Osterloh, F. E., Hydrogen evolution with fluorescein-sensitized Pt/SrTiO3 nanocrystal photocatalysts is limited by dye adsorption and regeneration. *Journal of Photochemistry and Photobiology A: Chemistry* **2020,** *400*, 112705.

41. Wuille Bille, B. A.; Kundmann, A. C.; Osterloh, F. E.; Velázquez, J. M., Ln10S14O (Ln = La, Pr, Nd, Sm) Oxysulfides: A Series of Direct n-Type Semiconductors. *Chem. Mater.* **2022,** *34* (16), 7553-7562.

42. Hamann, T. W.; Jensen, R. A.; Martinson, A. B. F.; Van Ryswyk, H.; Hupp, J. T., Advancing beyond current generation dye-sensitized solar cells. *Energy & Environmental Science* **2008,** *1* (1), 66-78.

43. Zhang, L.; Yang, X.; Wang, W.; Gurzadyan, G. G.; Li, J.; Li, X.; An, J.; Yu, Z.; Wang, H.; Cai, B.; Hagfeldt, A.; Sun, L., 13.6% Efficient Organic Dye-Sensitized Solar Cells by Minimizing Energy Losses of the Excited State. *ACS Energy Letters* **2019,** *4* (4), 943-951.

44. Hardin, B. E.; Snaith, H. J.; McGehee, M. D., The renaissance of dye-sensitized solar cells. *Nature Photonics* **2012,** *6* (3), 162-169.

45. Klahr, B. M.; Hamann, T. W., Current and Voltage Limiting Processes in Thin Film Hematite Electrodes. *J. Phys. Chem. C* **2011,** *115* (16), 8393-8399.

46. Wang, Q.; Hisatomi, T.; Suzuki, Y.; Pan, Z.; Seo, J.; Katayama, M.; Minegishi, T.; Nishiyama, H.; Takata, T.; Seki, K.; Kudo, A.; Yamada, T.; Domen, K., Particulate Photocatalyst Sheets Based on Carbon Conductor Layer for Efficient Z-Scheme Pure-Water Splitting at Ambient Pressure. *Journal of the American Chemical Society* **2017,** *139* (4), 1675-1683.